[37] E. S. Sabisky, Phys. Rev. **141,** 352 (1966).
[38] Z. J. Kiss, C. H. Anderson, and R. Orbach, Phys. Rev. **137,** A1761 (1965).
[39] E. S. Sabisky, J. Chem. Phys. **41,** 892 (1964).
[40] Z. J. Kiss and R. C. Duncan, Jr., Proc. IEEE **50,** 1532 (1962).
[41] E. Loh, Phys. Rev. **175,** 533 (1968).
[42] C. K. Asawa and R. A. Satten, Phys. Rev. **127,** 1542 (1962).
[43] S. Geshwind, G. E. Devlin, R. L. Cohen, and S. Chinn, Phys. Rev. **137,** A1087 (1965).
[44] G. F. Imbush and S. Geshwind, in *Optical Properties of Ions in Crystals*, edited by H. M. Crosswhite and H. W. Moos (Interscience, New York, 1967), p. 171.
[45] N. V. Karlov, J. Margerie, and Y. Merle-D'Aubigne, J. Phys. Radium **24,** 717 (1963).
[46] C. H. Anderson and E. S. Sabisky, Phys. Rev. **178,** 547 (1969).
[47] E. S. Sabisky and C. H. Anderson, Appl. Phys. Letters **13,** 214 (1968).

PHYSICAL REVIEW B VOLUME 2, NUMBER 11 1 DECEMBER 197

Dilute Cr^{3+} Paramagnetic Resonance in AlK Alum and $AlNH_4$ Alum*

PHILIP J. BENDT

Los Alamos Scientific Laboratory, University of California, Los Alamos, New Mexico 87544

(Received 13 July 1970)

Single-crystal Cr^{3+} paramagnetic-resonance spectra have been recorded at 1.3 K and ~19 kG for four sulfate alum crystals, in which the Al:Cr ratio varied from 215:1 to 590:1. The g value of the Cr^{3+} ions is independent of crystal orientation, and equals 1.977 ± 0.003. The zero-field Stark splitting $2D$ was measured for AlK alum (Al:Cr=435:1), and equals 0.011 cm^{-1}. The hyperfine coupling constant $|A|$ for ^{53}Cr was measured as $(1.6\pm0.05)\times10^{-3}$ cm^{-1}. The paramagnetic spectra are dominated by the $(-\frac{1}{2}, \frac{1}{2})$ transition, whose linewidth varied from 7 to 22 G. Spin-lattice relaxation is not strongly phonon bottlenecked, and the relaxation time varied from 2 to 3 msec at 0.95 K. With {111} planes perpendicular to the magnetic field, the $(-\frac{1}{2}, \frac{1}{2})$ resonance line is favorable for dynamic pumping of proton polarization.

I. INTRODUCTION

The electron-paramagnetic-resonance (EPR) spectra of Cr^{3+} ions in alums have been calculated and measured at room temperature.[1–3] Better-resolved spectra were obtained by diluting the chromium with diamagnetic aluminum.[2] Bleaney and Penrose[4,5] made measurements down to 20 K. The Cr^{3+} EPR spectra are discussed in two reviews.[6,7]

We have measured the Cr^{3+} EPR spectra of four alum crystals, in which the Al:Cr ratio varied from 215:1 to 590:1, as part of an investigation of the dynamic polarization of protons in alum.[8] The measurements were made in a ^4He cryostat between 1.0 and 1.3 K, and in a magnetic field between 18.5 and 19.5 kG. We measured the Cr^{3+} g value, the zero-field Stark splitting, the hyperfine coupling with the ^{53}Cr nucleus, the ion spin-lattice relaxation times, and the width and shape of the EPR lines. A full account of the polarization experiments is given in the following paper.

II. ALUM CRYSTALS

Single crystals of $AlK(SO_4)_2\cdot12H_2O$ and $AlNH_4(SO_4)_2\cdot12H_2O$ were grown from saturated solutions[9] at room temperature. The concentrations of chromium in the crystals, as determined by analysis,[10] were less than in the solutions, as shown in Table I. Crystals weighing several grams grew from seeds weighing 2–5 mG in about 10 days.

Each crystal was spectrographically analyzed for iron-group impurities. These were present in less than 5 ppm, with one exception: It was reported that $AlNH_4$ alum No. 4 contained approximately the same amount of Cu (100 ppm) as it did Cr. We searched for the paramagnetic Cu^{2+} resonance over a wide range of g values[11] with high sensitivity[12] without finding any indication that copper was present. However, the proton relaxation time was much shorter than in the other $AlNH_4$ alum (crystal No. 3).[13]

The crystal habit is to grow in the form of a regular octahedron, the large plane faces of which are equilateral triangles. The unit cell is cubic and the triangular faces are {111} planes. The angle between normals to adjacent triangular faces is 70° 32′. The density of the crystals was not measured; the handbook values are 1.757 (AlK) and 1.64 ($AlNH_4$).[14]

From the crystals, irregular cylinders were cut which contained two adjacent {111} faces as part of the

TABLE I. Crystals used in the EPR and dynamic-proton-polarization studies.

Crystal No.	1	2	3	4
Composition	AlK alum	AlK alum	$AlNH_4$ alum	$AlNH_4$ alum
Weight (mg)	460	501	330	290
Al:Cr ratio (solution)	200	70	100	100
Al:Cr ratio (crystal)	435	215	380	590
Measured g value (± 0.003)	1.976	1.978	1.977	1.977
Half-width δH of $(-\frac{1}{2}, \frac{1}{2})$ line (G)	10	7.5	11	5

"cylindrical" surface. The cylinders were ~1 cm long and ~0.6 cm in diameter. They were mounted in the microwave cavity as shown in Fig. 1, with the edge between {111} faces oriented vertically. The top view in Fig. 1 shows a {111} plane perpendicular to the **H** field,

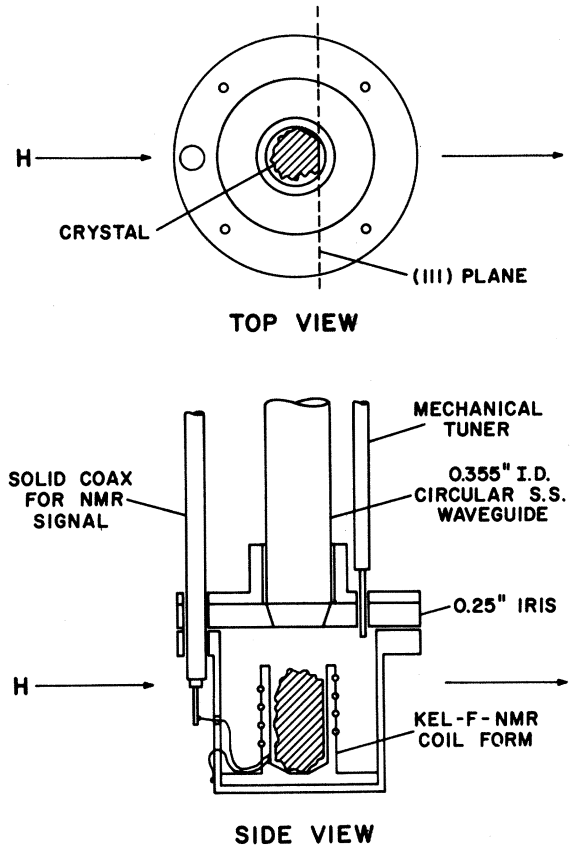

FIG. 1. Microwave cavity used for EPR measurements and dynamic proton polarization.

with the edge at the top of the figure. This was the first crystal orientation for which EPR spectra were obtained. The microwave cavity and crystal could be rotated about a vertical axis from outside the cryostat. Rotating the crystal 35° 16′ clockwise from the position shown in Fig. 1 orients the (110) planes perpendicular to the **H** field, for the second crystal orientation. Rotating the crystal 54° 44′ counterclockwise from the position shown in Fig. 1 orients the (100) planes perpendicular to the **H** field, for the third crystal orientation.

III. APPARATUS

The cryostat was a conventional batch-type ^4He cryostat connected through a 6-in.-diameter pumping line to a 750-liter/sec mechanical pump.[15] The lowest temperature which could be reached was 0.93 K. The alum crystal and microwave cavity were immersed in liquid helium. The cryostat insert, consisting of circular waveguide, cylindrical cavity, NMR coaxial cable, and cavity-tuning rod, could be rotated about a vertical axis. The microwave power dissipated in the cavity was measured from the increase in helium boil-off rate, with a gas-flow meter on the pump exhaust.

Magnetic field was provided by a 15-in.-pole-diameter electromagnet, which provided a field uniformity of about 0.1 G over the crystal volume. Field stability was maintained by a feedback circuit using a Hall-probe sensor.[16] The field strength was calibrated against the proton NMR frequency of 4.2577 kHz/G.

The cylindrical microwave cavity was machined from OFHC copper. The 0.25-in.-diameter iris shown in Fig. 1 was chosen to provide moderately high Q and good coupling to the waveguide. The mechanical tuning rod was used in connection with an oscilloscope display of cavity modes and could be used to spoil an unwanted overlapping mode, and occasionally to sharpen a wanted mode.

The cavity diameter was 2.045 cm, the length was 2.065 cm, and the volume was 6.78 cm^3. Since the wavelength of the microwaves was $\sim$0.56 cm, each linear dimension was about four wavelengths, and cavity modes were high-order modes. Since the crystal dimensions were one to two wavelengths, the crystal was uniformly irradiated with microwave power, except for nodes in the standing-wave pattern.

We made an analysis of resonances in the reflected microwave pattern displayed on an oscilloscope by sweeping the klystron reflector voltage, in the frequency range 52.5–53.1 GHz. The density of resonances was 25 per GHz, compared with a calculated density for the microwave cavity of 21 per GHz, using an acoustic formula.[17] A few of the observed resonances may have been in the waveguide instead of the cavity. The average width of strong resonances, such as we used, was $\sim$26 MHz at 52 GHz, indicating the cavity Q equaled $\sim$2000.

The microwave system outside the cryostat consisted of a 350-mW klystron,[18] isolator, calibrated attenuator, power meter, directional couplers, and a crystal diode detector.[19] The detector viewed the microwave power reflected from the cavity through a 10- or 20-dB directional coupler. Early in the experiments, we tried a microwave bridge using a hybrid tee. We found the added complexity of the bridge less satisfactory than direct observation of reflected power from the cavity.

EPR spectra were obtained by using the amplified output of the crystal detector to drive a strip-chart recorder while the magnetic field was swept at 100 G/min through resonance. It was necessary that the klystron frequency be locked to a cavity mode with a klystron stabilizer.[20]

The ion spin-lattice relaxation time was measured by the method of Baker and Ford,[21] using a microwave switch[22] which attenuated the power level by $\sim$50 dB.

IV. ANALYSIS OF REFLECTED MICROWAVE POWER

In this section, we show that direct observation of microwave power reflected from the cavity, when a stabilizer locks the klystron frequency to a cavity resonance, results in a signal proportional to the imaginary component of dynamic susceptibility. The dynamic susceptibility of the crystals is written $\chi=\chi'-i\chi''$. In order to show that $4\pi\chi''$ is $\ll 1$, we calculate its value for crystal No. 1. The first step is to calculate the static susceptibility χ_0 from Curie's law,

$$\chi_0=N(g\beta)^2I(I+1)/3kT, \tag{1}$$

where N is the number of Cr^{3+} ions in the sample, g is the ion g value, β is a Bohr magneton, I is the spin quantum number, k is Boltzmann's constant, and T is the temperature. Substituting N and g for crystal No. 1 and setting T equal to 1.3 K, we obtain χ_0 equal to 3.18×10^{-6} erg/G^2.

The relation between χ'' and χ_0 at resonance is[23]

$$\chi''=\tfrac{1}{2}\chi_0(\omega_0/\Delta\omega)=\tfrac{1}{2}\chi_0(H_0/\Delta H), \tag{2}$$

where ω_0 is the resonant frequency and $\Delta\omega$ is the half-width of the line; H_0 is the magnetic field at resonance; and ΔH is the half-width in G. Since $H_0/\Delta H$ equals 1.9×10^3, we obtain $4\pi\chi''=0.038$.

We now derive an expression for the reflected power from the microwave cavity. The admittance Y of the cavity is given by

$$Y=G+i(C\omega-1/L\omega), \tag{3}$$

where G is the conductance, C the capacitance, and L the inductance of an equivalent circuit. We write

$$L=L_c+L_s(1+4\pi\chi'-i4\pi\chi''), \tag{4}$$

where L_c is the inductance of the empty cavity and L_s is the inductance of the sample with the magnetic field off. We define $L_0=L_c+L_s$. Making use of the fact that $4\pi\chi''\ll1$, we obtain

$$Y=G+i\left\{C\omega-\frac{1}{[L_c+L_s(1+4\pi\chi')]\omega}\times\left(1+\frac{iL_s\omega4\pi\chi''}{[L_c+L_s(1+4\pi\chi')]\omega}\right)\right\}. \tag{5}$$

With the magnetic field off, we are tuned to a cavity resonance, so

$$C\omega-1/L_0\omega=0. \tag{6}$$

The factor $L_s(1+4\pi\chi')$ in Eq. (5) "pulls" the frequency of the cavity resonance as the magnetic field is swept through the EPR resonance. However, the function of the klystron stabilizer is to keep the klystron frequency equal to the cavity resonant frequency, even when the latter is "pulled." Thus we have

$$C\omega-[L_c\omega+L_s\omega(1+4\pi\chi')]^{-1}=0. \tag{7}$$

Noting that $4\pi\chi'$ is also small compared to 1, Eq. (5) reduces to

$$Y\approx G+(L_s/L_0^2\omega)4\pi\chi''. \tag{8}$$

The reflected power P_r is given by

$$P_r=\gamma^2P_0, \tag{9}$$

where γ is the reflection coefficient and P_0 is the incident power. The reflection coefficient of the cavity is

$$\gamma = |(Y-G_0)/(Y+G_0)|, \tag{10}$$

where $G_0=1/Z_0$ is the characteristic conductance of the waveguide. If we chose a cavity resonance for which the dip in the reflected power displayed on the oscilloscope went to the baseline, then we would have $G=G_0$. However, we chose resonances for which G was not equal to G_0. We define $\Delta G=G-G_0$. Dropping the small term in the denominator, we have

$$\gamma = \frac{\Delta G+(L_s/L_0^2\omega)4\pi\chi''}{G+G_0}. \tag{11}$$

Squaring Eq. (11) and dropping the small term in $(4\pi\chi'')^2$, we obtain

$$\gamma^2 = \left[\frac{\Delta G}{G+G_0}\right]^2 + \frac{2\Delta G(L_s/L_0^2\omega)4\pi\chi''}{(G+G_0)^2}. \tag{12}$$

We now substract the constant term, defining

$$\Delta P_r = P_0\{\gamma^2-[\Delta G/(G+G_0)]^2\}$$

$$= \frac{P_0 2\Delta G(L_s/L_0\omega)^2 4\pi\chi''}{(G+G_0)^2}. \tag{13}$$

The quantity ΔP_r is plotted in Figs. 3–7 and, within the limitations of this analysis, is proportional to χ''.

V. THEORETICAL Cr^{3+} EPR SPECTRUM

A cubic unit cell of α-alum contains four molecules, and has an edge length of 12.158 Å for the AlK alum and 12.240 Å for the $AlNH_4$ alum.[24] Each aluminum or chromium ion is surrounded by six octahedrally distributed water molecules, the Al-H_2O or Cr-H_2O spacing being about 2 Å.

The cubic crystal field at the Cr^{3+} ion, due to the surrounding water molecules, quenches the orbital angular momentum of the electrons, in the $^4F_{3/2}$ state. The symmetry of the crystal field is actually trigonal, there being a small cylindrical electric field in addition to the cubic field. There are four locations for Cr^{3+} ions in a unit cell, and the axes of the cylindrical fields at the different locations are parallel to different cube diagonals; i.e., they are perpendicular to the four {111} planes.

The Cr^{3+} ion has a spin $S=\frac{3}{2}$. The cylindrical fields cause a zero-field Stark splitting of the ground state into two levels, $\pm\frac{1}{2}$ and $\pm\frac{3}{2}$, separated by the energy $2D$. The Hamiltonian for the energy levels can be written

$$\mathcal{H} = g\beta\mathbf{H}\cdot\mathbf{S}+D[S_z^2-S(S+1)]+A\mathbf{S}\cdot\mathbf{I}, \tag{14}$$

where β is a Bohr magneton, A is the hyperfine coupling constant, and $\mathbf{I}$ is the nuclear spin ($I=\frac{3}{2}$ for ^{53}Cr). The first term gives the Zeeman levels in the applied field $\mathbf{H}$, the second term gives the fine structure due to Stark splitting, and the last term gives the hyperfine structure. The hyperfine interaction splits each transition into four equally spaced lines. Since the natural isotopic abundance of ^{53}Cr is 9.54%, the hyperfine lines are usually obscured by a broad line due to the even-even isotopes.

Taking account of the fine structure and the four ion

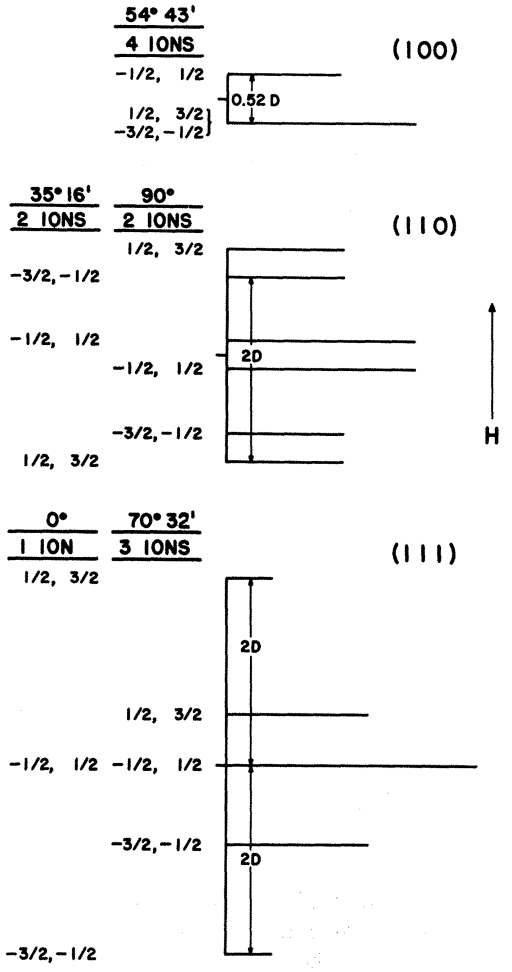

FIG. 2. Theoretical Cr^{3+} EPR spectra in alums, calculated for constant frequency, with magnetic field $\mathbf{H}$ increasing in the direction of the arrow. Spectra are shown for three crystal orientations, in which the (100), (110), and (111) planes are perpendicular to $\mathbf{H}$. The angles are between the magnetic field and the cylindrical crystalline fields. For the (110) and (111) orientations, there are two types of ions in a unit cell. The Zeeman levels involved in each transition are listed.

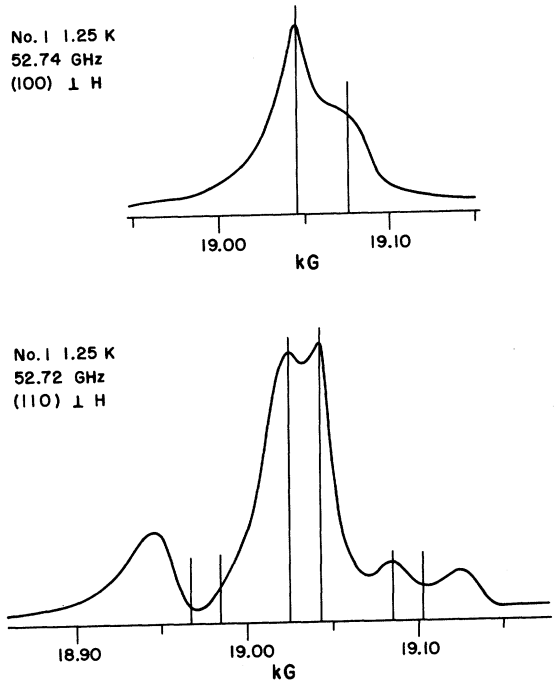

FIG. 3. EPR spectra of crystal No. 1 with the (100) and (110) planes perpendicular to the magnetic field **H**, taken with ~1 mW of microwave power. The lines locate theoretical transitions for zero-field splitting $2D$ equal to 0.011 cm^{-1}.

positions in a unit cell, Weiss[1,2] has calculated the EPR spectra for high magnetic fields for three crystal orientations, and these are shown in Fig. 2. The figure designates the Zeeman levels for each line, as well as showing the relative intensity and spacing of the lines.[25] Figure 2 applies to both AlK and $AlNH_4$ alums and to all Cr^{3+} concentrations, with the zero-field splitting $2D$ as a scale factor, to be determined by experiment. The splitting $2D$ depends both on Cr^{3+} concentration and temperature. Room-temperature measurements[3] confirm the calculated spectra.

The spectra in Fig. 2 are for "infinite" sample temperature. At the high magnetic field (19 kG) and low temperature (1.3 K) we used, each Zeeman level has six times the population of the next level above, in thermal equilibrium, due to the Boltzmann statistical factor. Under these experimental conditions, the spectrum in Fig. 2 is modified as follows: The $(\frac{1}{2}, \frac{3}{2})$ transition between the two highest Zeeman levels should not be experimentally observable, and $(-\frac{3}{2}, -\frac{1}{2})$ transition between the two lowest Zeeman levels should be enhanced by a factor of 6, relative to the $(-\frac{1}{2}, \frac{1}{2})$ transition.

In the (110) and (111) crystal orientations, the $(-\frac{3}{2}, -\frac{1}{2})$ lines are displaced by the Stark splitting from the center of the spectra, which occurs at the g value of the ion. Bleaney[4] has observed that the Stark splitting appears to be nonuniform throughout a dilute, mixed crystal at low temperature. Bleaney observed that the lines displaced from the center of the spectra were either split up or smeared out, and were weaker than given by theory. For this reason, the most intense lines correspond to the $(-\frac{1}{2}, \frac{1}{2})$ transition, despite the preferential occupation of the $-\frac{3}{2}$ Zeeman level.

VI. LOW-TEMPERATURE CHANGES IN ALUM

Bleaney[4] reported that CrK alum undergoes a phase transition when cooled down, which starts ~160 K, and continues over a broad temperature range. $CrNH_4$ alum has a somewhat sharper transition, which occurs at ~80 K. At temperatures below the transition, Bleaney interpreted the EPR spectra as showing two different Stark splittings. When optically clear $CrNH_4$ alum crystals were warmed to room temperature after being cooled to 20 K, it was found that a physical change had taken place: The crystals were opaque, as though shattered into an enormous number of microcrystals.

Bleaney reported that mixed crystals of $AlNH_4$ and $CrNH_4$ alum showed the phase transition if the Al:Cr ratio was 3:1, but did not show the transition for a ratio of 30:1. No mention was made of low-temperature spectra of dilute Cr^{3+} in AlK alum.

The alum crystals we used were optically clear when first put in the cryostat. After being cooled to 1.3 K and warmed again, the AlK alum was unchanged, but the $AlNH_4$ alum was opaque (white), as described above.

VII. EPR SPECTRA OF AlK ALUM

Low-power (~1-mW) EPR spectra of crystal No. 1 are shown in Figs. 3 and 4. The location of theoretical EPR lines from Fig. 2 are shown on these spectra. The extreme outside lines in the (110) orientation, and the lines on the high-field side of the (111) orientation, correspond to $(\frac{1}{2}, \frac{3}{2})$ transitions, and should not be observable due to depletion of the upper Zeeman levels. The best agreement is obtained for a zero-field Stark splitting $2D$ equal to 120 G, which corresponds to 332 MHz, or to 0.011 cm^{-1}.

There are no other measurements of the zero-field splitting for dilute Cr^{3+} ions in alums at low temperature. Bleaney[4] found the Stark splitting in undiluted CrK alum decreased steadily with decreasing temperature from 0.12 cm^{-1} at 290 K to 0.035 cm^{-1} at 160 K, above the phase transition. In the same crystal below the phase transition, Bleaney measured two splittings, 0.15 and 0.27 cm^{-1}, which did not change down to 20 K. Whitmer *et al.*[2] measured 0.091 cm^{-1} at room temperature in a mixed AlK and AlCr alum, which had an Al:Cr ratio of $8\frac{1}{2}$:1.

Figures 3 and 4 show that in a sufficiently dilute AlK alum (Al:Cr ratio=435:1), the theoretical spectrum

can still be identified at 1.25 K. The spectra of crystal No. 2 (Al:Cr ratio=215:1) closely resemble those of No. 1, except that the two central lines are not as well resolved in the (100) and (110) orientations. The spectra of crystal No. 2 are not sufficiently clear to make a reliable estimate of the zero-field splitting. The spectrum for the (111) orientation of crystal No. 2 is shown in Fig. 4, and the linewidth for the $(-\frac{1}{2},\frac{1}{2})$ transition in this orientation is somewhat narrower than for crystal No. 1.

We point out that the theoretical spectra can be obtained only if the crystal orientation with respect to the magnetic field is rather precise. We could determine the orientation of the crystal from outside the cryostat to $\pm 2°$, and more exact orientation was obtained by making several recordings of the EPR spectra, each at a slightly different setting.

The (111) orientation of the AlK alums was used for dynamic-proton-polarization experiments, and while the lines are wider than for the $AlNH_4$ alums, the AlK alums polarize satisfactorily. We also used the central peak of the EPR spectra in the (111) orientation to make precise measurements of the g value of the Cr^{3+} ions. The values obtained, listed in Table I, average to 1.977 ± 0.003. No dependence of the g value on crystal orientation was detected.

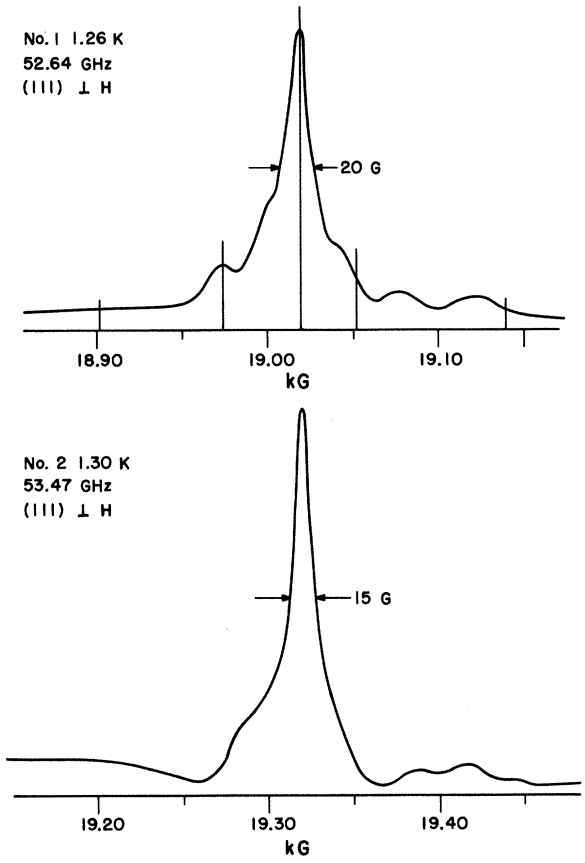

FIG. 4. EPR spectra of crystals Nos. 1 and 2 with the (111) plane perpendicular to the magnetic field **H**, taken with ~1 mW of microwave power. The lines in the top figure are for zero-field splitting $2D$ equal to 0.011 cm^{-1}.

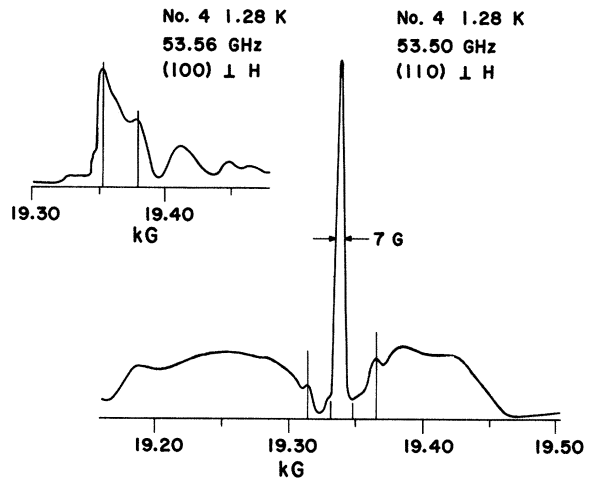

FIG. 5. EPR spectra of crystal No. 4 with the (100) and (110) planes perpendicular to the magnetic field **H**, taken with 10-mW microwave power. The lines in the (100) orientation correspond to zero-field splitting $2D$ equal to 0.0097 cm^{-1}. The lines in the (110) orientation show the location of the hfs lines of ^{53}Cr.

VIII. EPR SPECTRA OF $AlNH_4$ ALUMS

The EPR spectra of $AlNH_4$ crystal No. 4 are shown in Figs. 5 and 6. A very narrow line corresponding to the $(-\frac{1}{2},\frac{1}{2})$ transition was observed in two crystal orientations. When a sharp, narrow line was observed, it was flanked by small satellite peaks. These are the two outside hyperfine-structure lines of ^{53}Cr, which was present in its natural isotopic abundance of 9.54%. From the 52-G separation of these lines, we were able to calculate the absolute value of the coupling constant A in Eq. (14). We obtain $|A| = (1.6\pm 0.05)\times 10^{-3}$ cm^{-1}.

Bleaney and Bowers[26] have determined the hyperfine coupling constant of ^{53}Cr, using a sample of deuterated potassium chromium selenate alum, isotopically enriched to 97% ^{53}Cr. They established unambiguously that the nuclear spin of ^{53}Cr is $\frac{3}{2}$. The value for $|A|$ they obtained was $(1.85\pm 0.1)\times 10^{-3}$ cm^{-1}, which differs from our measurement by more than the combined experimental errors. Comparing the figure of hyperfine-structure lines Bleaney and Bowers published with our figures leads us to conclude the splitting can be measured more precisely from our EPR spectra than from the earlier experiment.

All three spectra of crystal No. 3 were about 500 G wide, or twice as wide as the spectra of the AlK alums. They were dominated by the $(-\frac{1}{2},\frac{1}{2})$ transition, but the spectra did not resemble the theoretical spectra.

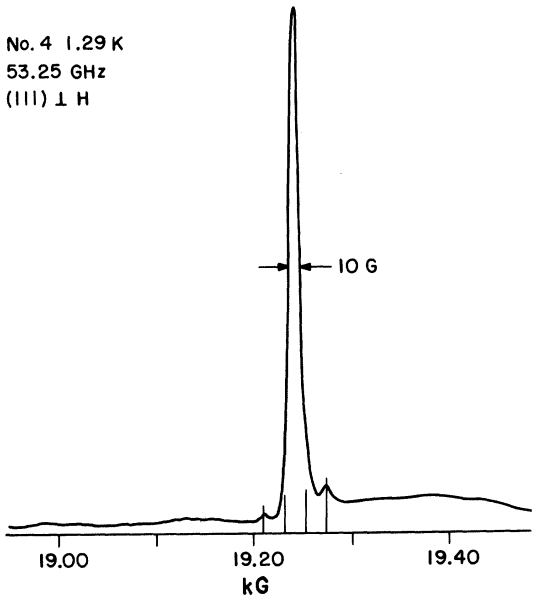

FIG. 6. EPR spectra of crystal No. 4 with the (111) plane perpendicular to magnetic field **H**, taken with 10 mW of microwave power. The lines locate the hfs lines of ^{53}Cr.

Two spectra of crystal No. 3 taken with the (111) plane perpendicular to the magnetic field are shown in Fig. 7. The upper spectrum was taken with ~1 mW of microwave power, and the lower spectrum (recorded with lower amplifier gain) was taken with 200 mW of microwave power. The line corresponding to the $(-\frac{1}{2}, \frac{1}{2})$ transition is only $\frac{1}{3}$ as wide when recorded at the higher power.

The narrowing of the EPR line at high power is not understood. If the diode detector response had changed from square law at low power to linear in voltage at high power, the line would have appeared wider rather than narrower.

Nearly all the microwave power is absorbed in the crystal at the center of the EPR line. When the resonance was recorded at 200 mW, the crystal was heated briefly at a rate of ~1 W/cm^3. The temperature rise in the crystal was estimated to be 1 K at the surface due to Kapitza resistance, and 2 K more from the outside to the center of the crystal, due to thermal resistance. Since the magnetic field sweep was comparatively slow (200 G/min for Fig. 7), the crystal temperature was probably higher while the central EPR line was recorded than it was while the wings were recorded.

We were unable to interpret the $AlNH_4$ alum spectra in terms of the theoretical spectra. This is not surprising, since Bleaney found the $CrNH_4$ alum spectra to be anomalous at low temperature. Describing the spectrum below the phase transition, Bleaney wrote[4]: "The spectrum cannot be observed during the transition, but subsequently the spectrum is found to be quite different from that above the transition point, and it cannot be fitted to a normal spectrum for any value of the splitting. This spectrum remains substantially unaltered on cooling to liquid hydrogen temperatures."

Considering the possibility that in a dilute $AlNH_4$ crystal some vestige of the theoretical spectrum remains, we note that the narrow spectrum in the (100) orientation would be least affected by nonuniformity of the crystalline fields throughout the sample. We have accordingly calculated the zero-field splitting which would give rise to the two lines drawn on the (100) spectrum of crystal No. 4 (Fig. 5), and obtain $2D = 105$ G, corresponding to 290 MHz, or 0.0097 cm^{-1}. This value is close to that obtained for AlK crystal No. 1, but is not confirmed by the spectra at other orientations.

We used the (111) crystal orientation to polarize protons in crystal No. 3, and both the (110) and (111) orientations to polarize in crystal No. 4. Rapid polarization growth rates were observed with both these crystals. The g values we measured in $AlNH_4$ alums are listed in Table I.

IX. SPIN-LATTICE RELAXATION TIMES

We measured the spin-lattice relaxation time T_{1e} of Cr^{3+} in the four alum crystals, and of Nd^{3+} in a sample

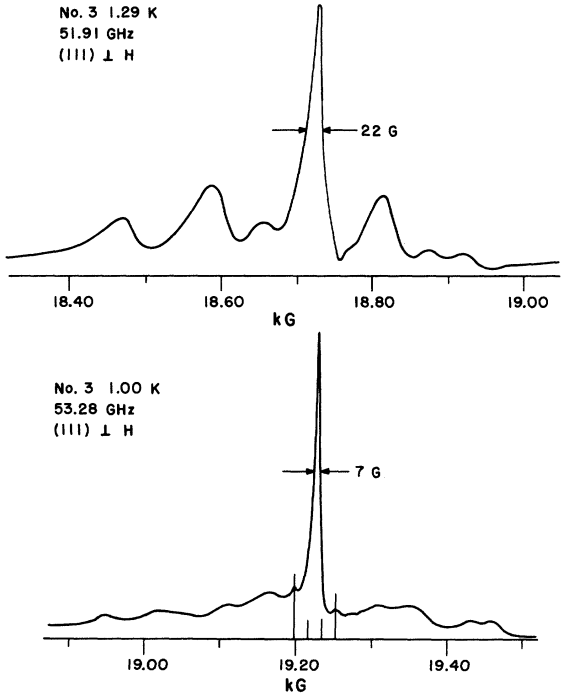

FIG. 7. EPR spectra of crystal No. 3 with the (111) plane perpendicular to the magnetic field **H**. At the top is the low-power spectrum (~1 mW) and below is the high-power spectrum (~200 mW). The lines locate the hfs lines of ^{53}Cr.

of lanthanum magnesium nitrate (LMN).[27] We used the method of Baker and Ford,[21] in which the electron-resonance signal recovers from saturation while the microwaves are turned off. The microwave power used to saturate the electron resonance varied from 0.12 to 0.15 W, and since the microwave switch attenuated by somewhat more than 50 dB, the sample was irradiated with 1 ± 0.3 μW while the relaxation was measured. The extent to which transitions induced by 1 μW affect the measured value of T_{1e} is not known. In addition, the precision with which we could measure T_{1e} was rather low: ±0.4 msec for the alums and ±1 msec for LMN.

Spin-lattice relaxation times have been studied much more extensively in LMN than in the alums. Below 1.5 K, the Raman and Orbach processes are negligible in LMN,[28] and T_{1e} can be expressed by[21]

$$T_{1e}=[A(h\nu/2k)\coth(h\nu/2kT)]^{-1}+[B(h\nu/2k)^2\coth^2(h\nu/2kT)]^{-1}, \quad (15)$$

where h is Planck's constant, k is Boltzmann's constant, and ν is the microwave frequency. A and B are coefficients, and B is expected to be proportional to the width of the EPR line.[28] The linewidth itself is often proportional to the frequency. The first term in Eq. (15) represents the direct process, and the second term results from slowing down the direct process by a phonon bottleneck. Spin-lattice relaxation in LMN is not phonon bottlenecked at low magnetic fields,[28] but at 14 kG and 1 K, the second term in Eq. (15) is $\sim$20 times as large as the first term.

We measured T_{1e} in LMN, with the c axis perpendicular to the magnetic field, at two temperatures. Assuming T_{1e} is due entirely to the second term in Eq. (15), we solved for B. The results for T_{1e} and B are given in Table II. Baker and Ford obtained $B=16$ at 16.6 GHz; Scott and Jeffries obtained $B=35$ at 35 GHz. Our measurements of B at 54 GHz show that B continues to increase with frequency.

The T_{1e} measurements of the alum crystals are given in Table III. We do not have an equation comparable to Eq. (15) for the alums. We can only make the following comments: (a) T_{1e} in the alum crystals at $\sim$54 GHz and 0.96 K is roughly four times shorter than in LMN for the same conditions. (b) The temperature dependence of T_{1e} in the alum crystals between 0.96 and 2 K is much weaker than given by the phonon-bottleneck term in Eq. (15), and is in better agreement with the temperature dependence of the direct process. From these results we conclude that the usual direct process is dominant in alums.

TABLE II. Results of T_{1e} measurements on LMN at 53.92 GHz and 14.26 kG. B is a constant in Eq. (15), and $h\nu/2k=1.294$ K.

Temperature (K)	T_{1e} (msec)	$\coth(h\nu/2kT)$	$B(s^{-1}K^{-2})$
0.93	11.5	1.132	40.5
1.35	7.0	1.353	46.6

TABLE III. Measurements of T_{1e} of the alum crystals.

Crystal	AlK No. 1	AlK No. 2	$AlNH_4$ No. 3	$AlNH_4$ No. 4
Magnetic field (kG)	19.35	18.83	19.58	19.55
Frequency (GHz)	53.56	52.13	54.18	54.10
T_{1e} (msec) at 0.96 K	2.5	2.0	3.0	2.8
T_{1e} (msec) at 2.00 K	1.9	1.6	2.2	2.0
$T_{1e}(0.96)/T_{1e}(2.00)$	1.32	1.25	1.36	1.40

The saturation factor for EPR is given by

$$S=T_{1e}T_{2e}(\gamma_e H_{1e})^2, \quad (16)$$

where T_{2e} is the transverse relaxation time, γ_e is the gyromagnetic ratio, and H_{1e} is the microwave field inducing transitions. For T_{2e} we use the expression $T_{2e}=(\gamma_e\delta H)^{-1}$, where δH is the half-width at half-power of the $(-\frac{1}{2},\frac{1}{2})$ transition, measured with low microwave power ($\delta H=3$ G in LMN). The steady-state dynamic proton polarization depends on S through the factor $S/(S+S_{1/2})$, where $S_{1/2}$ is a constant depending on crystal properties and the magnetic field. The measured values of $T_{1e}T_{2e}$ were 7 to 15 times smaller in alums than in LMN, which makes S smaller for the same microwave power, by Eq. (16). The dynamic-proton-polarization experiments reported in the following paper show that, due to the shorter ion relaxation times, it takes three times as much microwave power in alums as in LMN to obtain the same value of $S/(S+S_{1/2})$.

ACKNOWLEDGMENTS

We are grateful for valuable discussions with Dr. L. J. Campbell, Dr. H. G. Hecht, and Dr. C. F. Hwang, and to Dr. W. B. Lewis for reviewing this manuscript. We express our thanks to Dr. J. E. Simmons, Dr. J. A. Jackson, and J. C. Martin for assistance with equipment.

* Work performed under the auspices of the U.S. Atomic Energy Commission.

[1] P. R. Weiss, Phys. Rev. **73,** 470 (1948); C. Kittel and J. M. Luttinger, *ibid.* **73,** 162 (1948).

[2] C. A. Whitmer, R. T. Weidner, J. S. Hsiang, and P. R. Weiss, Phys. Rev. **74,** 1478 (1948).

[3] D. M. S. Bagguley and J. H. E. Griffiths, Proc. Roy. Soc. (London) **A204,** 188 (1950).

[4] B. Bleaney, Proc. Roy. Soc. (London) **A204,** 203 (1950).

[5] B. Bleaney and R. P. Penrose, Proc. Phys. Soc. (London) **60,** 395 (1948).

[6] B. Bleaney and K. W. H. Stevens, Rept. Progr. Phys. **16,** 108 (1953).

[7] W. Low, in *Solid State Physics*, edited by F. Seitz and D. Turnbull (Academic, New York, 1960), Suppl. 2.

[8] P. J. Bendt, Phys. Rev. Letters **25,** 365 (1970).

[9] The AlK, CrK, and $AlNH_4$ sulfates used to make the solutions were Baker Analyzed Reagent, J. T. Baker Co., Phillipsburg, N.J. The manufacturer's analysis stated the Fe impurity was 50 ppm in the CrK sulfate and 5 ppm in the other two. The $CrNH_4$ sulfate was reagent grade supplied by City Chemical Corp., New York, with no accompanying analysis.

[10] The aluminum concentrations were determined gravimetrically, and the chromium concentrations were determined by atomic absorption in a flame, using the 3578.7-Å chromium line. The concentrations were measured by Ross Gardner, Group CMB-1, Los Alamos Scientific Laboratory.

[11] The g value of Cu^{2+} in $Cu(NH_3)_4(SO_4)\cdot H_2O$ varies from 2.02 to 2.15, according to T. Okamura and M. Date, Phys. Rev. **94,** 314 (1954). The value 2.02 places the Cu^{2+} resonance 400 G below the Cr^{3+} resonance, when the latter is at 18.5 kG.

[12] For the same linewidth, we would have detected a Cu^{2+} resonance 1/50 as intense as the Cr^{3+} resonance.

[13] The proton relaxation time T_{1p} was 3350 sec in crystal No. 3 and 1350 sec in crystal No. 4, at 0.93 K.

[14] *Handbook of Chemistry and Physics*, 50th ed., edited by R. C. Weast (Chemical Rubber Publishing Co. Cleveland, Ohio, 1969).

[15] Stokes model 1722-S (Pennsalt Chemicals Corp.).

[16] Magnet control was by a Varian Fieldial Mark I, which also provided magnetic field sweep.

[17] P. M. Morse and K. U. Ingard, *Theoretical Acoustics* (McGraw-Hill, New York, 1968), p. 587, Eq. (9.5.12). The formula for $dN/d\nu$ was multiplied by 2 for the two polarization directions of transverse waves.

[18] Varian of Canada VC-104, which operated between 51.8 and 54.2 GHz.

[19] Microlab/FXR crystal detector, part No. Z-227-S. This is a square-law detector in the power range in which we used it (<1 mW).

[20] Teltronics model KSLP.

[21] J. M. Baker and N. C. Ford, Phys. Rev. **136,** A1692 (1964).

[22] TRG model V-120, Control Data Corp.

[23] A. Abragam, *The Principles of Nuclear Magnetism* (Oxford U. P., London, 1961), p. 43.

[24] R. W. G. Wyckoff, *Crystal Structures*, 2nd ed. (Interscience, New York, 1960), Vol. 3, p. 872.

[25] The line intensities for the (110) plane perpendicular to **H** were not published by Weiss. Those shown in Fig. 2 are from an experimental measurement by Bagguley and Griffiths (Fig. 6 of Ref. 3).

[26] B. Bleaney and K. D. Bowers, Proc. Phys. Soc. (London) **A64,** 1135 (1951).

[27] The LMN crystal was grown by the late Dr. T. R. Roberts. A nominal 1% of the La was replaced with "unenriched" Nd. Dynamic proton polarization in the LMN crystal was compared with that obtained in the alum crystals, and a measurement of T_{1e} was needed to calculate the saturation factor. All measurements on LMN were made with the c axis perpendicular to the magnetic field ($g=2.70$).

[28] P. L. Scott and C. D. Jeffries, Phys. Rev. **127,** 32 (1962).